Hydrometallurgy 169 (2017) 142–151

Contents lists available at ScienceDirect

Hydrometallurgy

journal homepage: www.elsevier.com/locate/hydromet

Influence of physicochemical properties of Brazilian serpentinites on the leaching process for indirect CO_2 mineral carbonation

Gretta L. A. F. Arce [a,b,*], Turibio G.S. Neto [a], I. Ávila [b], Carlos M.R. Luna [b], José C. dos Santos [a], João A. Carvalho Jr [b]

[a] Combustion and Propulsion Associated Laboratory, Brazilian Space Research Institute (LCP/INPE), Brazil
[b] Combustion and Carbon Capture Laboratory, Energy Department, São Paulo State University (LC3/DEN/UNESP), Brazil

ARTICLE INFO

Article history:
Received 23 May 2016
Received in revised form 10 November 2016
Accepted 21 January 2017
Available online 24 January 2017

Keywords:
Serpentinite
Leaching
Physicochemical properties
Indirect mineral carbonation
Reactivity

ABSTRACT

pH-swing mineral carbonation is kinetically favorable and requires a short reaction time. It must also obtain a high extraction rate for reactive elements in the leaching process. The main purpose of this study is to investigate the behavior of different serpentinite rocks in the leaching processes; the reactivity of Brazilian serpentinite rocks (such as: S-GO and S-MG) is analyzed based on physicochemical properties in order to understand their relationship to leaching efficiency. Surface area-to-volume ratio (S_{BET}/V_p) and metals-to-silicon ratio (Σ(Mg, Ca)/Si) were used to measure reactivity. Leaching was carried out to determine Mg and Fe extraction. Reaction conditions for both serpentinite rocks were: 355–250 μm particle size, 4 M HCl concentration, 100 °C, and 2 h of reaction time. Characterization results show that both serpentinite rocks (S-GO and S-MG) have high magnesium (Mg) content. S_{BET}/V_p was 36 for S-GO and 29 for S-MG, while Σ(Mg, Ca)/Si was 2.64 for S-GO and 1.20 for S-MG. These results suggest that S-GO is approximately 50% more reactive than S-MG, and that S-MG is limited by low accessible surface (S_{BET}/V_p) and the high mineralogical complexity (Σ(Mg, Ca)/Si). Leaching results confirmed the reactivity; Mg and Fe extraction from S-GO was 94 ± 1%. However, results for S-MG were 34% for Mg and 60% for Fe. In order to increase the reactivity of S-MG, particle size was reduced to 75–63 μm. Even though S-MG was mechanically activated, Mg and Fe extraction has not increased significantly.

1. Introduction

Carbon dioxide (CO_2) emission from fossil fuel combustion is the greatest factor in the current increase in atmospheric CO_2 concentration. The concentration of CO_2 in the atmosphere reached 401 ppm in 2016 (Arce et al., 2014; Edenhofer et al., 2014). Due to the growing worldwide demand for energy, fossil fuel will continue to be the major source of energy in the near future. Fossil fuels have many advantages, principally its high energy density and low operating cost (Olajire, 2013).

Carbon Capture and Storage by Mineralization (CCSM) is a safe technology that is known to store CO_2 permanently in the form of environmentally stable carbonates (Gadikota et al., 2014a; Sanna et al., 2014a, 2014b, 2013a; Styles et al., 2014). Today, there are two types of CCSM approaches: i) in situ or direct mineral carbonation; and ii) ex-situ or indirect mineral carbonation. Indirect mineral carbonation could make a great contribution to CO_2 storage; however, there are many challenges to implement it on an industrial scale (Chang et al., 2012; Gadikota et al., 2015; Hemmati et al., 2014a; Sanna et al., 2013b; Styles et al., 2014).

There have been several studies on indirect mineral carbonation in which the highest carbonation efficiencies were obtained through the pH-swing method (Dri et al., 2013; Hemmati et al., 2014a; Sanna et al., 2013a, 2013b; Teir et al., 2007b). As stated by Hemmati et al. (2014b), this method is kinetically favorable and requires a short reaction time. It also allows the separation and recovery of products with a high level of purity (silica, iron oxides and carbonates) that could be potentially used in a wide range of sectors, hence reducing the emissions from production of such materials (Alexander et al., 2007; Azdarpour et al., 2015; Bobicki et al., 2012; Sanna et al., 2013a, 2013b, 2012). Nonetheless, due to the high cost of the process, it will not be economically feasible for CO_2 storage without considering the utilization of such products (Hemmati et al., 2014a).

Lately, indirect mineral carbonation has focused on using silicate rocks because they are common throughout the world. However, the pH-swing method did not have good kinetics for all silicate rocks. In many cases, the lowest extraction rate of the reactive elements was reached (Mg, Ca, and Fe) (Daval et al., 2013; Meyer et al., 2014; Park and Fan, 2004; Sanna et al., 2014a; Sanna et al., 2013a, 2013b; Van Essendelft and Schobert, 2010). Since this method is quite costly, it must obtain a high extraction rate of reactive elements. Thereby, the

* Corresponding author at: Brazilian Space Research Institute (INPE), Combustion and Propulsion Associated Laboratory (LCP), Rodovia Presidente Dutra, km 40, Cachoeira Paulista, SP CEP 12630-000, Brazil.
E-mail addresses: grettagaf@yahoo.es, gretta@lcp.inpe.br (G.L.A.F. Arce).

http://dx.doi.org/10.1016/j.hydromet.2017.01.003
0304-386X/

reactivity of silicates rocks must be carefully assessed. A detailed appraisal may greatly improve CCSM efficiency (Erlund et al., 2016; Gadikota et al., 2014b; Styles et al., 2014).

Currently, researchers have many challenges. One of the most important is to improve the reactivity of these silicate rocks in order to reduce the energy requirement and, consequently, the cost involved in the process (Bobicki et al., 2015; Fricker and Park, 2013; Hemmati et al., 2014b; Lackner et al., 1995; Meyer et al., 2014; Olajire, 2013; Park and Fan, 2004; Sanna et al., 2014b; Sanna et al., 2013a, 2013b; Wang and Maroto-Valer, 2011a, 2011b). For these reasons, pretreatment methods found in other published studies for indirect mineral carbonation, are being combined, such as mechanical activation, thermal activation, and chemical treatment.

While there have been many studies in this field, there is still a discrepancy regarding CO_2 capture potential of silicate rocks. In order to get a better understanding of whether or not silicate rocks are adequate, recently Gadikota et al. (2014b); Lacinska et al. (2016); Lavikko and Eklund (2016); Styles et al. (2014) have suggested that silicate rocks must be characterized more carefully because their mineralogy varies widely. The characterization must consider pore structure, surface area (S_{BET}), origin, subsequent metamorphic changes, and crystal structure of the minerals in the rocks.

According to Assima et al. (2014), when reactivity is considered, materials for direct mineral carbonation based on carbonation potential (R_{CO2}) are not similar. This is due to the fact that reactivity is the product of physicochemical properties. In pH-swing mineral carbonation, the selection of materials is still realized on carbonation potential (R_{CO2}) proposed by Goff et al. (2000) which was based strictly on their Mg, Ca, and Fe contents. It is worth mentioning that rocks contain several minerals in their structure, which can cause the rock to be more or less reactive. This means that the reaction condition may not be similar for all materials. Therefore, to assess the reactivity of the material for indirect mineral carbonation, Mg, Ca, and Fe contents, and other important criteria such as Si content, crystal structure, and textural properties, which are intrinsically related, must also be considered.

The main objective of this study was to investigate the behavior of different types of Brazilian serpentinite rocks on leaching for their use in pH swing mineral carbonation. The reactivity of serpentinite rocks is analyzed based on physicochemical properties. Thus textural properties, mineral composition, and crystal structure are studied, as well as the surface area-to-volume ratio (S_{BET}/Vp) and metals-to-silicon ratio (Σ(Mg, Ca)/Si) were used, in order to understand their interrelationship with leaching efficiency.

2. Materials and methods

2.1. Materials

Two types of serpentinite rock (S) were chosen for this study. A *waste rock* of the asbestos fiber production from Minaçu Mine was selected, located in Cana Brava in the state of Goiás in Brazil. This rock was identified as S-GO. The other serpentinite was a rock from a factory that mines serpentinite for industrial use from Nova Lima mine located in the state of Minas Gerais in Brazil. This rock was identified as S-MG. Both S-GO and S-MG were provided in the form of rocks, and their average dimensions were 31.0 × 15.5 cm and 15.0 × 10.0 cm. See Fig. A1a (S-GO) and b (S-MG).

A ball crusher was used in order to reduce their size. S-GO and S-MG were ground in a jar mill with alumina spheres of different sizes. Calcined alumina spheres were used since they have a hardness of approximately 9 mohs. Particle size was classified for characterization analysis after the material was ground, using an ASTM 200 mesh (75 μm) and a 230 mesh (63 μm), so that the fraction had grains between these two sizes. For the leaching experimental test, two particle sizes were used. Thus, to obtain average particle sizes of 69 μm (63–75 μm) and 302 μm (250–355 μm), ASTM mesh numbers 230–200 and 45–60 were used, respectively.

2.2. Characterization methods

Samples of each serpentinite rock were prepared and underwent the following analyses: Hg intrusion porosity (MIP); N_2 adsorption surface area; thermogravimetric analysis (TGA); X-ray diffraction (XRD); Scanning electron microscope with dispersive X-ray energy spectrometry (MEV-EDS); wavelength dispersion sequential fluorescence (XRF); and inductively coupled plasma optical emission spectroscopy (ICP-OES).

Mercury intrusion porosimetry (MIP) and N_2 adsorption surface area are well known techniques that have been used to analyze the structure and volume of pores (micro, meso, and macropores). They can evaluate factors such as fluid and ion permeability within particles (Das et al., 2014; Ramli et al., 2013; Zeng et al., 2014). Pore structure, macropore volume, and porosity of materials were determined through MIP analysis in a series 33 PoreMaster. Before being tested, materials were dried in an oven for 12 h at 100 °C. After being dried, 250 ± 10 mg samples were collected in a P/N 74122 penetrometer with 2 mm D.I. and 0.5 cm^3 vol. Afterwards, a NOVA series Micrometromics Quantacroms N_2 adsorption surface area measurer was used to evaluate BET surface area and volume of mesopores. 170 ± 10 mg samples were inserted into the analyzer cell. The samples then underwent a thermal surface cleaning treatment at 200 °C for 3 h in primary vacuum.

Thermogravimetric analyses (TGA) were carried out to assess the thermal behavior of both serpentinite rocks and residues obtained after the leaching process. These TGA were carried out in a TA Instrument SDT TGA-DSC Q600 simultaneous system. The sample mass used was approximately 30 ± 2 mg, with a 5 × 5 mm alumina crucible employed for all tests. A dynamic nitrogen atmosphere was applied as purge gas, using 100 mL/min flow rate and 10 °C/min heating rate. Temperatures were set between 30 and 1000 °C.

Mineralogical composition was determined using a PANalitical X'pert3 Powder model X-ray diffraction analyzer (XRD). This device uses Cu Kα radiation in a range of 6–90 °2θ. Diffractograms obtained were processed using the HighScore Plus software. A mass of approximately 1 ± 0.5 g was used for this analysis.

SEM-EDS analysis was carried out to determine the materials' morphology and elemental distribution. A Zeiss EVO LS 15 equipped with an EDS/EBDS Oxford INCA Energy 250 system (Oxford Instruments, Abingdon, Oxfordshire, UK) was used for the scanning electron microscope analysis. Dispersive energy microanalysis was executed. It operated between 0.2 and 30 kV and employed an Everhart-Thornley secondary electron detector, 8.5 mm away from the samples.

Sequential fluorescence with wavelength dispersion (XRF) was used for quantitative analyses of chemical composition of the materials. It was carried out using a PANalytical Axios MAX-Advanced model, a device with 4.0 kW operating power and 60 kV agitation. This analyzer was used to perform a quantitative elemental chemical analysis of boron (B) and uranium (U). For this analysis, a 1 ± 0.2 g sample of each material was used.

ICP-OES analyses were conducted to determine elemental composition with an Arcos Spectro model inductively coupled plasma optical emission spectroscope. A 250 ± 10 mg powder sample of each material was employed.

2.3. Leaching experimental tests

To evaluate the influence of the physicochemical properties on leaching processes, the same reaction conditions were employed for S-GO and S-MG. The reaction conditions considered were stoichiometric mass/volume ratios, 250–355 μm particle size, 4 M HCl concentration, and 100 °C temperature.

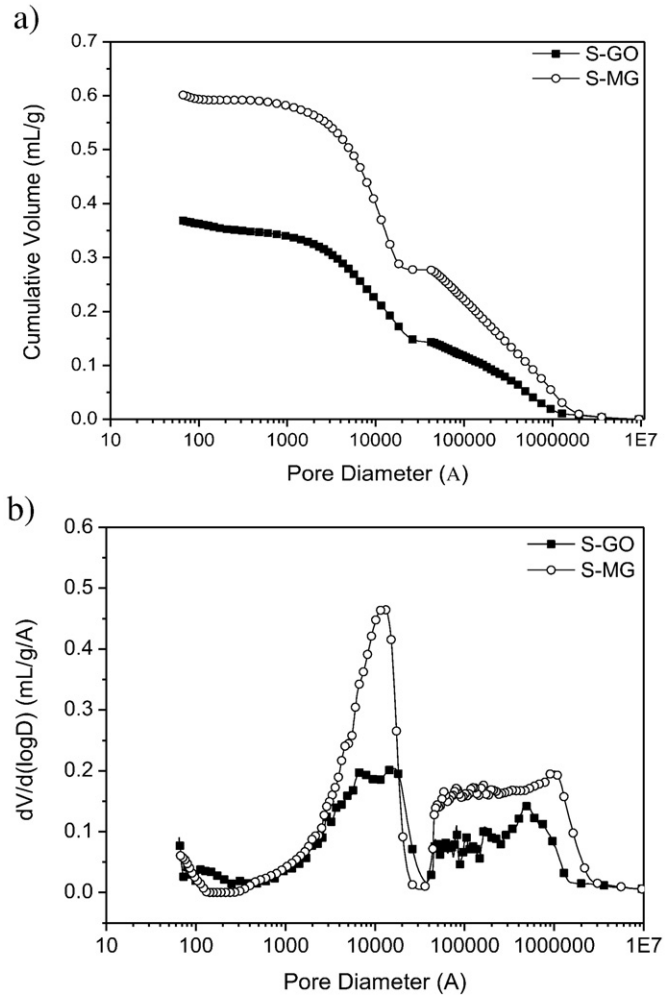

Fig. 1. Mercury porosity analysis of the two different serpentinite rocks: (a) Cumulative intrusion volume curve; (b) Curve of the difference of V by the difference of the Log of pore diameter.

Stoichiometric mass/volume ratios for the experimental tests were 146 g/L for S-GO and 168 g/L for S-MG. Initially, acid solutions were inserted into a 500 mL vessel reactor and heated to a specified temperature. Once the acid solution was heated, the powder was added to the vessel reactor, which was equipped with a Graham condenser to avoid HCl loss by evaporation, as well as a thermocouple for temperature control; it was continuously agitated with a magnetic stirrer set at 600–700 rpm. The leaching process was maintained for 2 h based on other studies (Hemmati et al., 2014a; Teir et al., 2007b; Van Essendelft and Schobert, 2009).

After each leaching experimental test (T), two products were obtained: a precipitate or solid residue (R) and a leachate solution (L). The precipitate was separated from the liquid through vacuum filtration. Following each experiment, residues (R) were dried for 2 h at 105 °C. Then, TG/DTG and XRD analyses were carried out in order to observe the structural modifications from serpentinite rocks after the leaching process.

Leachate solutions (L) were analyzed by ICP-OES to obtain Mg, Fe, and Si concentrations and to determine extraction percentage. Mg, Fe, and Si extractions in the leachate solution (L) were calculated based on their "*in natura*" contents within serpentinite rocks, according to the following equations, from Eqs. (1) to (3):

$$X_{Mg} = \frac{V_{SOL} \times C_{Mg}}{M_t \times Mg\%_{M_t}} \times 100 \quad (1)$$

$$X_{Fe} = \frac{V_{SOL} \times C_{Fe}}{M_t \times Fe\%_{M_t}} \times 100 \quad (2)$$

$$X_{Si} = \frac{V_{SOL} \times C_{Si}}{M_t \times Si\%_{M_t}} \times 100 \quad (3)$$

In which: X represents the percentage of the element extracted; Mg%, Fe%, and Si% are the initial element contents in the serpentinite sample; M_t is the initial mass of sample used in the experiments; V_{SOL} is the leachate solution volume after 2 h of reaction; C_{Mg}, C_{Fe}, and C_{Si} are the concentrations of the elements in the leachate solution.

3. Results and discussion

3.1. Physicochemical characterization

MIP and N_2 adsorption techniques were used to obtain the textural properties of each serpentinite rock in order to evaluate factors such as fluid permeability within particles (Das et al., 2014; Ramli et al., 2013; Zeng et al., 2014). The MIP result is obtained as pore size distribution (PSD), which is shown in the form of cumulative volume intrusion curves (Fig. 1a) and volume intrusion curves (Fig. 1b).

Cumulative volume intrusion curves (Fig. 1a) have two distinct regions: the first region is interparticle volume, and the second region is intraparticle volume. In order to evaluate the volume of fluid that was introduced into the material, cumulative intrusion volumes of the intraparticle region (IV_I) have to be considered. Table 1 also shows that S-MG has an IV_I average value of around 0.36 mL/g, while S-GO has a lower value of 0.17 mL/g.

The intrusion volume differential curve (Fig. 1b) shows PSD in greater detail. Three regions can be seen in each sample. The intraparticle region is divided into a macroporous and a mesoporous region. Although both serpentinite rocks contain macro and mesopores, the mesoporous region has lower pore volume. The size of the macroporous region indicates that S-MG has greater pore volume than S-GO.

Fig. 1b also shows that for both serpentinite rocks, there is an increase in pore volume in the mesoporous region. The N_2 adsorption technique was used to determine pore volume (20–500 Å) and BET surface area (S_{BET}), respectively. Table 1 shows these results, in which S-GO has less pore volume in the mesoporous region. The BET surface area (S_{BET}) for S-MG is approximately 63% greater than the S_{BET} for S-GO.

Table 2 and Fig. 2 show the mineral phases found in both serpentinite rocks. The main phase of S-GO is lizardite 1T (L); the secondary phases are brucite (B), clinochrysotile (C), magnesite (m) and magnetite (M). The main phases of S-MG are antigorite (A) and talc

Table 1
Data calculated from Hg intrusion and N_2 adsorption curves for the materials.

Materials	IV_T (mL/g)	IV_I (mL/g)	S^b_{BET} (m^2/g)	V_p (mL/g)	
				20–500 Å[b]	500–40,000 Å
S-GO	0.38	0.17	6.8	0.012	0.17
S-MG	0.62	0.36	11.1	0.024	0.36

IV_T: total cumulative intrusion volume; IV_I: Intraparticle cumulative intrusion volume, S_{BET}: BET surface area; V_p: Total pore volume, [b]N_2 adsorption technique carried out with 250 ± 50 mg of material.

Table 2
Composition of Brazilian serpentinite rock mineral phases in XDR results.

Materials	Ref. code	Mineral name	Compound name
S-GO	00-050-1625	Trigonal Lizardite 1T	Aluminum Iron Magnesium silicate
	00-027-1275	ClinoChrysotile	Magnesium Silicate Hydroxide
	01-083-0114	Brucite	Brucite
	01-075-1609	Magnetite	Magnetite
	01-086-2345	Magnesite	Magnesium carbonate
S-MG	00-052-1573	Antigorite Monoclinic P	Magnesium Silicate Hydroxide
	00-011-0386	Lizardite 1T	Magnesium Aluminum Silicate Hydroxide
	00-029-1493	Talc 2M	Magnesium Silicate Hydroxide
	00-004-0594	Actinolite	Calcium Magnesium Iron Silicate Hydroxide
	00-024-0512	Chromite	Iron Chromium Oxide

(T), and the secondary phases are lizardite 1T (L), actinolite (a) and chromite (Ch). These mineralogical differences show that S-GO is derived from the hydration of dunites (olivine), however, S-MG is derived from hydration of pyroxenes (orthopyroxenes). This explains why there is brucite in S-GO, and actinolite and talc in S-MG. When the serpentinization process takes place at low temperature and pressure, serpentines can co-exist with silicon-free brucites ($Mg(OH)_2$), as shown in Eq. (4) (Evans, 2008; Frost et al., 2013; Frost and Beard, 2007). According to Styles et al. (2014); Frost and Beard (2007), pyroxene hydration processes in isothermal (400–500 °C) and isobaric conditions lead to the equimolar production of serpentines and talc (Eq. (5)). While temperature and pressure are important in the formation of rocks, the activity of silica ($aSiO_2$) is even more important. Serpentinization processes are carried out at high water activity levels (aH_2O) and low silica activity levels ($aSiO_2$); However, when $aSiO_2$ increases, the serpentines can form more complex minerals, as shown in Eq. (6) (Frost and Beard, 2007; Moore and Rymer, 2007; Power et al., 2013; Styles et al., 2014).

$$2\,Mg_2SiO_4 + 3H_2O \rightarrow Mg_3Si_2O_5(OH)_4 + Mg(OH)_2 \quad (4)$$

$$6\,MgSiO_3 + 3H_2O \rightarrow Mg_3Si_2O_5(OH)_4 + Mg_3Si_4O_{10}(OH)_2 \quad (5)$$

$$Mg_3Si_2O_5(OH)_4 + 2\,SiO_2 \rightarrow Mg_3Si_4O_{10}(OH)_2 + H_2O \quad (6)$$

In Figs. 3 and 4, note the micrographs of S-GO and S-MG, as well as the elemental distribution of magnesium (Mg), silicon (Si), aluminum (Al), chrome (Cr), total iron (Fe_t). Fig. 3a and b, shows the elemental distribution of Mg and Si, which are uniformly distributed across the micrograph of S-GO, showing the strong connection between them linked to the serpentines, in this case: lizardite 1T and clinochrysotile.

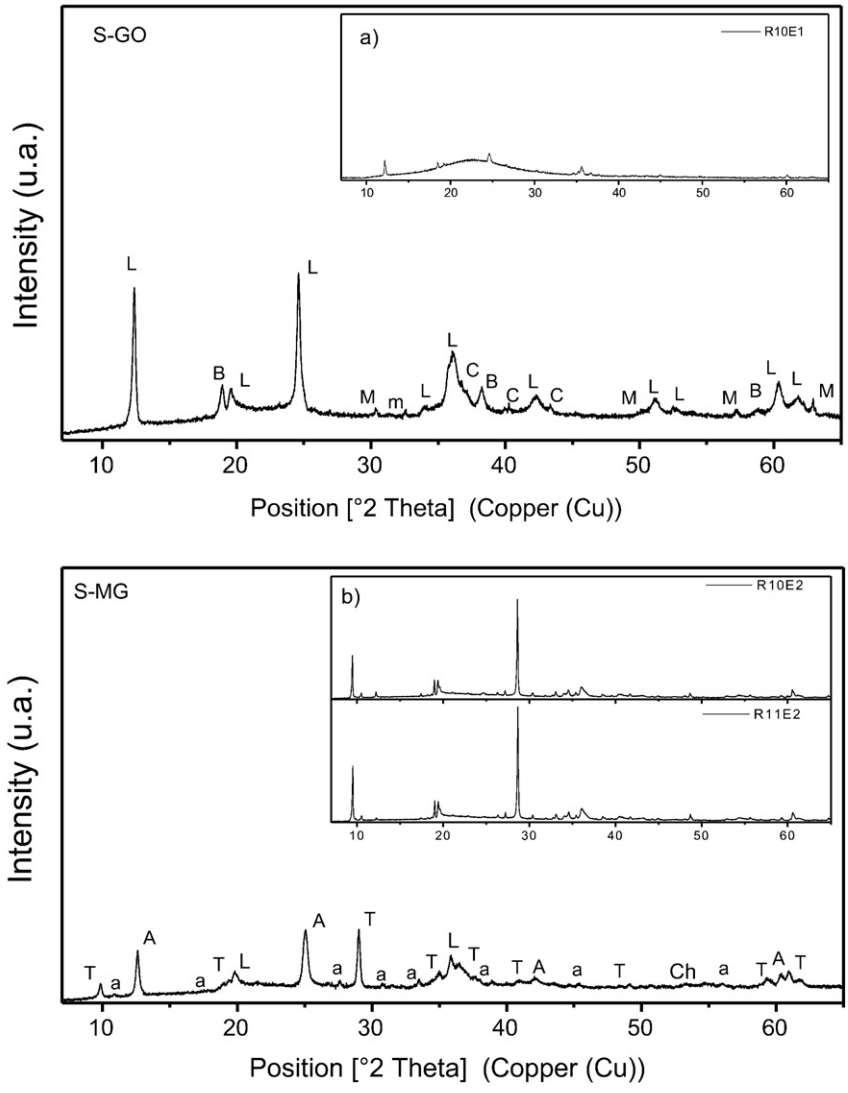

Fig. 2. X-Rays diffractograms for S-GO and S-MG "*in natura*". a) XRD for residue (R) after S-GO leaching, b) XRD for residues after S-MG leaching.

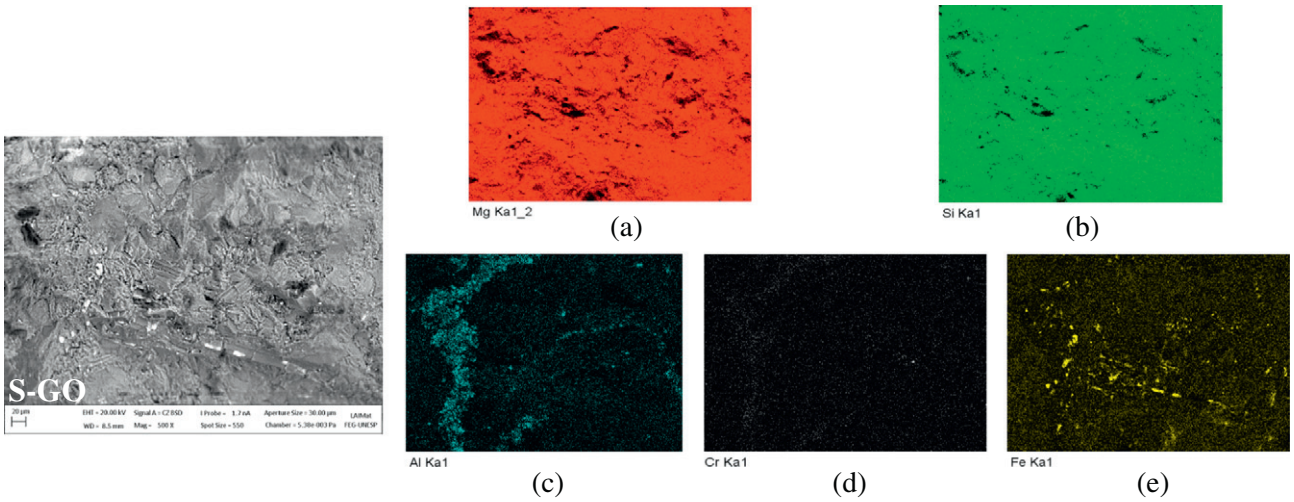

Fig. 3. Micrograph and elemental distribution of S-GO. a) magnesium (Mg), b) silicon (Si), c) aluminum (Al), d) chrome (Cr) and e) total iron (Fe).

In Fig. 3c, d and e, show that the elemental distribution of Al, Cr and Fe_t is in specific regions of the S-GO micrograph. Lizardites has a great affinity for cationic substitution of trivalent elements in the tetrahedral Si^{4+} sheet (T), causing the formation of ordered and flat structures (Wicks and Whittaker, 1975). This suggests that Al^{3+} and Cr^{3+} are found in the place of Si^{4+} in the T sheets, specifically in lizardite 1T. Fig. 3e shows a few specific points at which Fe_t has a high concentration due to the magnetite found in S-GO.

Fig. 4a,b and c, show the elemental distribution of magnesium (Mg), silicon (Si) and aluminum (Al) for S-MG. Note that the distribution of Al is uniform across the micrograph, just as Mg and Si are, though at a lesser concentration. According to the positioning of the elements, Al^{3+} seems to be linked to Mg^{2+} and Si^{4+}, consequently silicate minerals such as antigorite, lizardite 1T and/or talc might have substituted Al^{3+} for Si^{4+} in the sheet T. According to Wicks and Whittaker (1975), substitution of trivalent elements (Al^{3+} and Fe^{3+}) in antigorite is limited due to the curvature needed to produce octahedral sheets (O) which are larger than tetrahedral sheets (T), like chrysotiles, though at a lower intensity. On the other hand, Putnis (2003); Rayner and Brown (1973) pointed out that a large number of silicates with flat structures can result from the replacement of Al^{3+} for Si^{4+} in T sheets. Thus talc and lizardite 1T (contained in S-MG) might have carried out the substitution. Note that Cr and Fe_t are distributed in specific zones (Fig. 4d and e). This pattern is associated with chromite ($(Fe,Cr)_2O_4$) found in S-MG.

A thermogravimetric analysis (TGA) was performed in order to characterize the thermal decomposition of each mineral contained in both serpentinite rocks. Fig. 5a and b shows TG/DTG curves for S-GO and S-MG (black dotted line). A total mass loss of approximately 15.5% was observed for S-GO and 9.0% for S-MG, between 30 and 1000 °C. Different DTG peaks were found (Fig. 5b), which coincided with the weight lost (Fig. 5a).

Three minerals phases were identified on DTG curve for S-GO, which were associated with specific decomposition temperatures (Fig. 5b). DTG peaks at 382 °C indicated brucite dehydroxylation. Larger DTG peaks found at 600 °C and 659 °C indicated lizardite 1T and clinochrysotile dehydroxylation, respectively. Four minerals phases were identified on DTG curve for S-MG associated with specific decomposition temperatures (Fig. 5b). Larger DTG peaks indicated dehydroxylation of lizardite 1T at 637 °C and antigorite at 776 °C. Smaller DTG peaks indicated dehydroxylation of actinolite at 800 °C and talc at 900 °C.

Chemical and elemental composition determined by XRF and ICP-OES analyses is presented on Table 3. This table shows that S-MG has the highest SiO_2 content. S-GO and S-MG have significantly different SiO_2 contents, which can be explained by the fact that S-MG contains talc and actinolite (Fig. 2). ICP-OES analyses corroborate the difference in silicon (Si) between serpentinite samples. Table 3 also shows that there are higher levels of MgO in S-GO than S-MG. This is again

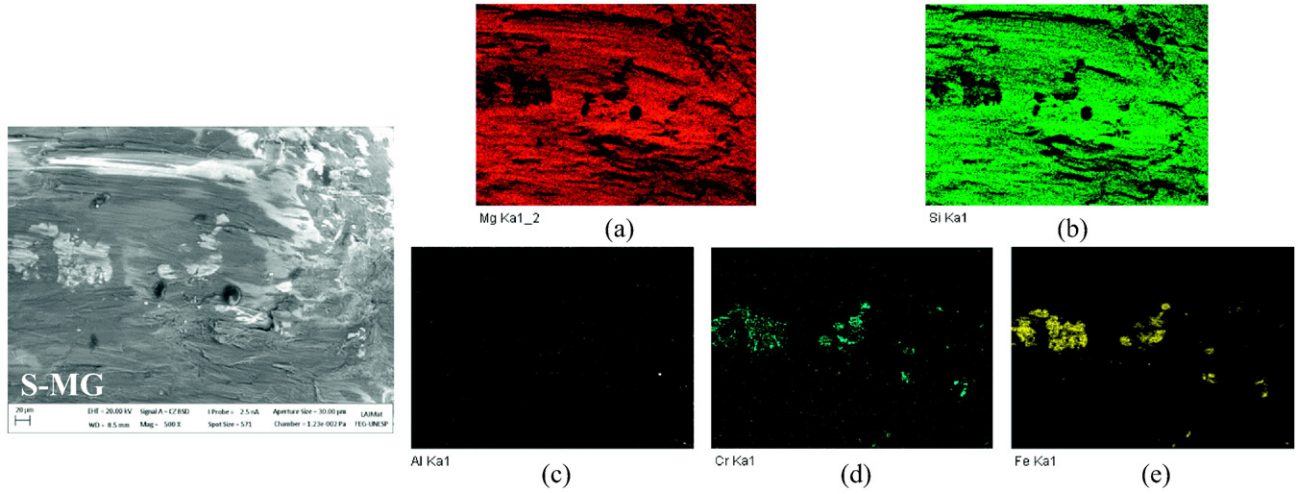

Fig. 4. Micrograph and Elemental distribution of S-MG. a) magnesium (Mg), b) silicon (Si), c) aluminum (Al), d) chrome (Cr) and e) total iron (Fe).

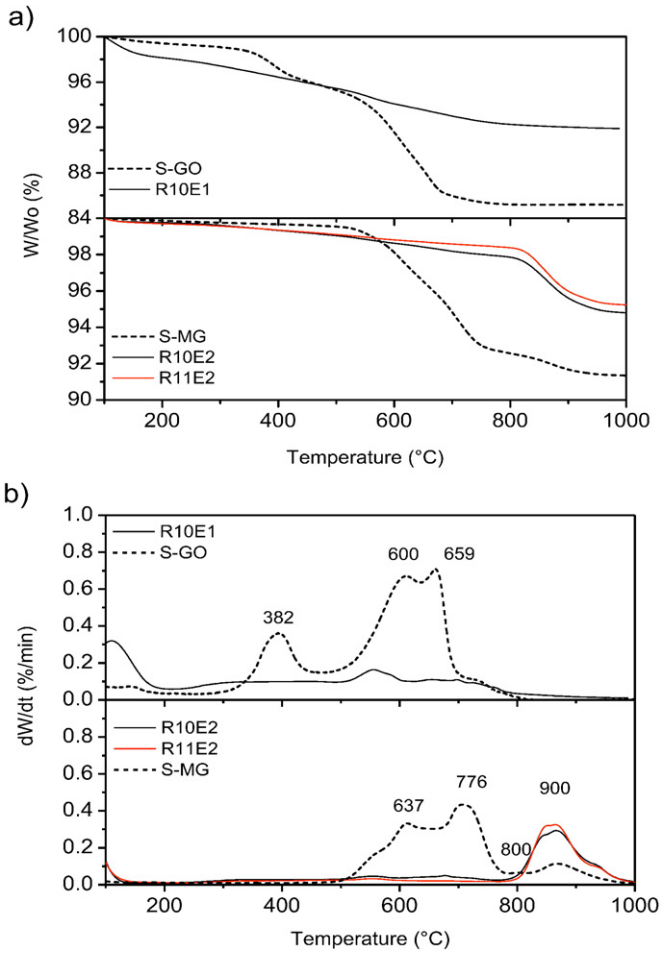

Fig. 5. Thermal decomposition of S-GO, S-MG and residues. a) TG curves, b) DTG curves.

corroborated by the Mg quantification through ICP-OES analysis; it is probably because S-GO contains brucite, which is known to be rich in Mg (Fig. 2).

3.2. Leaching experimental tests

Leaching experiments were performed in order to confirm the reactivity of S-GO and S-MG. Leachate solutions (L) for S-GO and S-MG were yellow and green-yellow, respectively. The solid residue (R) was slightly gray for both serpentinite rocks. Mg, Fe, and Si extractions found in the leachate (L) are shown on Table 4.

Table 3
Chemical and elemental composition in % w/w.

Oxides[a]	S-GO	S-MG	Elements[a]	S-GO	S-MG
SiO_2[c]	40.64	52.09	Si[c]	8.40	15.26
MgO[c]	43.33	30.63	Mg[c]	23.01	17.69
CaO	0.10	1.66	Ca	279.5[d]	0.70
Fe_3O_4[c]	12.61	11.82	Fe[c]	4.49	3.66
K_2O	n.d.	n.d.	K	<0.01[d]	<0.01[d]
Na_2O	n.d.	n.d.	Na	<0.02[d]	<0.02[d]
Al_2O_3	1.17	2.36	Al	0.35	0.96
TiO_2	n.d	0.08	Ti	140.3[d]	266.5[d]
MnO	0.20	0.27	Mn	737.8[d]	812.8[d]
Cr_2O_3	1.02	0.86	Cr	0.45[d]	0.219
LOI	15.5	9.0	R_{CO2} (t_{MAT}/t_{CO2})[b]	1.84	2.42

[a] Oxides were determined by XRF analysis and elemental contents were determined by ICP-OES.
[c] For calculation of Mg, Fe, and Si concentrations in the leachate (L), mean values of XRF and ICP-OES were used.
[b] Calculated by the method proposed by Goff et al. (2000).
[d] mg/kg, n.d. = not determined.

Table 4
Mg, Fe, and Si extracted from S-GO and S-MG in the leaching process.

Test	Reaction conditions			Extraction of metals in leached solutions (L)		
	ϕ (μm)	C_{HCl} [M]	T (°C)	Mg %	Fe %	Si %
T10E1	355–250	4	100	95	93	3
T10E2	355–255	4	100	34	60	2
T11E2	75–63	4	100	36	71	1

The experiments that used S-GO obtained the highest Mg and Fe extraction, of approximately 94 ± 1% (T10E1). Nonetheless, under the same conditions, maximum Mg and Fe extractions from S-MG reached only 34% and 60% respectively (T10E2). In order to increase Mg and Fe extraction, rocks underwent rigorous grinding, thus the particle size was reduced from 355 to 250 μm until 75–63 μm. Experimental test T11E2 was then performed. As can be seen on Table 4, Mg and Fe extraction reached approximately 36% and 71%, respectively.

Thermogravimetry and XRD analyses were performed on the residues (Figs. 5 and 2) in order to understand the mechanisms involved in the Mg and Fe extraction step and the interrelation between mineral structure and extraction performance for S-GO and S-MG. TG/DTG profiles were compared for S-GO and S-MG as well as the residues (Fig. 5), identifying if there was a partial or total reaction of each mineral contained in them. DTG peaks of the minerals that are still part of the residues can be seen on Fig. 5b, which illustrates the differences between *"in natura"* serpentinite rock peaks (S-GO and S-MG) and the residues (R) obtained after the leaching process.

Large differences for DTG peaks were identified between all residues and both "*in natura*" serpentinite rocks (Fig. 5b). DTG curves for R10E1 (leaching using S-GO) showed that the characteristic peaks of lizardite 1T (600 °C) were less intense than S-GO peaks from this region. However, brucite (382 °C) was not totally extracted. The diffractogram for R10E1 (Fig. 2a) reveals that there is significant structural modification consistent with the production of amorphous silica which is formed after the bonds between octahedral and tetrahedral sheets are broken in the serpentines, in which siloxanes (Si – O – Si) are encapsulated and precipitated as silica (Arce et al., 2017; McCutcheon et al., 2015; Sanna et al., 2013a, 2013b; Park and Fan, 2004). However, the diffractogram also shows that a large amount of the material has been transformed into amorphous silica, while non-reactive lizardite (L) and brucite (B) are still present.

Fig. 5b shows the R10E2 DTG curve for the S-MG leaching process. The characteristic peaks for lizardite 1T (637 °C) and antigorite (776 °C) were less intense than for S-MG peaks from this region. Talc was not extracted; moreover, its characteristic DTG peak (900 °C) was more intense. The high intensity of the DTG peaks indicated that antigorite and lizardite 1T were released from the structure, leaving the talc more exposed to thermal decomposition, so that their DTG peaks was more intense. The diffractogram of R10E2 (Fig. 2b) shows that most of the antigorite and lizardite 1T were removed from the structure. However, peaks for talc (T) also increased significantly in intensity (Fig. 2b). When the R11E2 DTG curve was assessed (red line), it was nearly the same as R10E2, corroborating ICP-OES results. The leaching process using S-MG extracted 36% of Mg. The sources of this Mg were the serpentines. Mg from talc is more difficult to extract because of its mineralogical complexity.

Talc (T) and actinolite (a) are more resistant to leaching than serpentines because of their crystalline structure. Talc is derived from the hydration of pyroxenes; in addition, the crystalline structure of both minerals is made up of tetrahedral (T) and octahedral (O) sheets organized in 2:1 flat layers, in which octahedral Mg^{2+} is encapsulated in two sheets of tetrahedral Si^{4+}. This characteristic helps to prevent the

bonds between the O - T sheets from breaking, making it harder to release octahedral Mg^{2+} (Temuujin et al., 2002).

Baba et al. (2015) and Temuujin et al. (2002) reported that 62% and 64% of talc was removed from the structure of the rock in 2 M HCl, 75 °C, particle size of 75 μm and 4 M H_2SO_4, 80 °C, unknown particle size, respectively. However, in our study, talc was seen to remain in the structure of S-MG (Fig. 2b). S-MG is highly resistant to leaching due to structural stability of talc given by Al^{3+} in the T sheet.

3.3. Reactivity by physicochemical properties

3.3.1. Surface area-to-volume ratio (S_{BET}/V_p)

Gadikota et al. (2014b) claimed that reactivity is strongly affected not only by rock heterogeneity, but also by the pore structures and surface area (S_{BET}). In chemical reactions involving solid materials, surface area-to-volume ratio is an important parameter because it employs textural properties of materials to estimate their reactivity. As pointed out by Klobes et al. (2006), porous materials with large surface area-to-volume ratios have often exhibited enhanced chemical reactivity. In addition, in many practical applications exploiting this large ratio, the size of the accessible surface is as important as the chemical composition.

Recent reports have shown that one of factors for slow kinetics in CO_2 mineralization is related to the low accessible surface (surface area – to – volume ratio) of the materials (Oskierski et al., 2013; Ukwattage et al., 2015; Yuen et al., 2016). when surface area – to – volume ratio value are low, the material is less permeable to fluid, which can limit the process of diffusion into the materials (Ukwattage et al., 2015; Yuen et al., 2016).

In this manner, the larger the accessible surface is, the more reactive the material becomes, although this depends on the material's physical structure. In this study, the S_{BET}/V_p ratio was calculated using Eq. (7), in which S_{BET} is the BET surface area and V_p is the total pore intraparticle volume.

$$r = \frac{S_{BET}}{V_p} \tag{7}$$

3.3.2. Metals – silicon ratio ($\Sigma(Mg, Ca)/Si$)

The reactivity also will depend on the mineralogical complexity which is linked to silica activity ($aSiO_2$). Beyond of temperature, pressure, water activity (aH_2O) and oxygen fugacity (fO_2), the silica activity ($aSiO_2$) is one of the most important parameters used in the classification of igneous rocks (Evans, 2008; Frost and Beard, 2007; Putnis, 2003).

As earlier mentioned, several minerals can co-exist with the serpentines, and mineralogical complexity is proportional to silica activity ($aSiO_2$) (Evans, 2008; Faust and Fahey, 1962; Frost et al., 2013). According to Oskierski et al. (2013), low MgO/SiO_2 ratios are related to silicified and weathered serpentinites. The silicification stage is accompanied by a gain in SiO_2 and losses of MgO and CaO, while early stages of weathering normally cause pores to develop (Oskierski et al., 2013).

Some authors state that mineralogical complexity is inversely proportional to reactivity. For example, minerals hydrated from dunites (olivine Mg_2SiO_4) have lower Si content in the structure than minerals hydrated from pyroxenes ($MgSiO_3$ and $(Mg,Ca)SiO_3$) (Styles et al., 2014). Thus, serpentinite rocks derived from dunites are more reactive for indirect mineral carbonation (Lavikko and Eklund, 2016; Styles et al., 2014). Assima et al. (2013) also reported that serpentinite rocks with higher Mg/Si molar ratio are more efficient for atmospheric CO_2 capture.

The reactivity based on mineralogical complexity should be assessed, using Mg, Ca, and Si ratios. Thus, due to the large mineral complexity of rocks, a mass ratio of these elements was considered for this study, as shown in Eq. (8).

$$r = \frac{\sum (Mg, Ca)}{Si} \tag{8}$$

Table 5
Σ(Mg, Ca)/Si and S_{BET}/Vp ratios for serpentinite rocks.

Parameters	S-GO	S-MG
S_{BET}/V_p	36	29
Σ(Mg, Ca)/Si	2.64	1.20

3.3.3. Reactivity of serpentinine rocks

Elemental composition, MIP, and N_2 adsorption results from Tables 1, 2 and 3 were used in Eqs. (7) and (8) to determine S_{BET}/V_p and Σ(Mg, Ca)/Si ratios, which are shown on Table 5. Although S-GO and S-MG have similar R_{CO2} (Table 3), Σ(Mg, Ca)/Si results suggest that S-GO is a less complex rock because it has a higher value than S-MG.

An increase in Σ(Mg, Ca)/Si ratio, is only possible when a serpentinite rocks contains *Si*-free magnesium and/or minerals with low levels of Si. S-GO had a high level of this ratio due to the presence of brucite ($Mg(OH)_2$). The structure of S-GO is made up of 6.1% brucite (Arce et al., 2017). Although this quantity isn't very high, this mineralogical characteristic makes S-GO more efficient at leaching than S-MG.

In contrast, while S-GO has a lower BET surface area (S_{BET}) than S-MG, the S_{BET}/V_p results indicated that S-GO has a larger accessible surface for reaction in leaching. A greater value would indicate more permeability at the beginning of the reaction to any fluid within the material. This is interesting because it could explain the high extraction rate reported by Arce et al. (2017), in which 88 ± 2% of Mg and Fe were extracted from S-GO in the first 30 min of the reaction.

Both mineralogical and textural characteristics of S-GO indicate that it is more reactive. The S_{BET}/V_p ratio shows the behavior of the diffusion processes and the Σ(Mg,Ca)/Si ratio indicates the mineralogical complexity of the serpentinite rocks. Nonetheless, there are other parameters such as chemistry and crystal structure that should be taken into consideration.

Considering both serpentinite rocks, it can be verified that S-GO is twice as reactive as S-MG. S-MG is more stable because of the high level of Al^{3+} in the T sheets of talc. It also is more limited by diffusion between silica hydrated layers formed on the leaching, and then, due to greater mineralogical complexity. Moreover, mechanical activation did not have a significant effect in this particular case. Therefore, more intensive mechanical activation and/or more active acids could be applied to S-MG in order to increase leaching efficiency, though this would make the process more costly. On the other hand, due to the chemical characteristics of S-GO, more intensive mechanic activation was not needed. This will reduce the energy consumption on the pretreatment method, and less active acid can be used.

3.4. Comparison of results obtained with published data

Based on results obtained, a comparison was made with data from previously published studies on Mg extraction efficiency, physicochemical properties, and reaction conditions, as shown on Table 6 and Fig. 6.

Different results from several published studies could be explained by Σ(Mg,Ca)/Si ratio values, as showed on Table 6. Several studies have used serpentinite (Daval et al., 2013; Park and Fan, 2004; Styles et al., 2014; Teir et al., 2007b; Wang and Maroto-Valer, 2011b), nonetheless, Mg extraction in function of Σ(Mg,Ca)/Si ratio varied a lot, as shown in Fig. 6 (black point). This behavior may have been caused by polymorphism and the crystal structure of serpentinites (chrysotile, antigorite, and lizardite).

When other silicate rocks were used, such as the pyroxenes and amphiboles shown on Table 6 (Meyer et al., 2014; Sanna et al., 2014a,

Table 6
Published results for the leaching process in indirect mineral carbonation.

Silicate rocks	Minerals	% Mg Extracted	Acid	Conditions	Characteristics					Parameters		References
					BET m^2/g	PS μm	Mg %	Ca %	Si %	Σ(Mg,Ca)/Si	R_{CO2}	
[1] Pyroxenes[a]	Orthopyroxenes Plagioclases	5	HCl	2 M,70 °C,8 h	n.r.	283	16.3	0.4	25.7	0.65	3.33	(Meyer et al., 2014)
[2] Serpentinite	Lizardite	9	HCl	1 M,90 °C,2 h	7.2	500–800	24.5	n.r.	19.7	1.24	2.26	(Daval et al., 2013)
[3] Olivine	Forsterite lizardite	98	HCl	1 M,100 °C,6 h	n.r.	<56	28.17	0.29	19.96	1.43	1.95	(Hemmati et al., 2014b)
[4] Serpentinite	Antigorite	40	HCl	1 M, 70 °C,5 h	4.2	37	27,1	n.r.	20.1	1.35	2.04	(Park and Fan, 2004)
[5] Serpentinite[b]	Chrysotile	100	HCl	2 M,70 °C,2 h	27.9	75–150	21.83	0.34	11.59	1.61	2.51	(Teir et al., 2007a)
	antigorite	80		2 M,70 °C,2 h	n.r.	300–500						
	lizardite											
[6] Amphibole	Actinolite prehnite clinochlore	30	NH_4HSO_4	1.4 M,100 °C,3 h	n.r	75–150	7.3	10.6	21.5	0.84	4.02	(Sanna et al., 2014a)
[7] Pyroxenes	Diopsite forsterite enstatite	30	NH_4HSO_4	1.4 M,100 °C,3 h	n.r	75–150	12.4	12.3	23.0	1.07	2.78	
[8] Serpentinite	Antigorite forsterite	98	NH_4HSO_4	1.4 M,100 °C,3 h	n.r.	75–150	24.28	0.07	17.81	1.37	2.28	(Wang and Maroto-Valer, 2011a)
[9] Olivine	Forsterite enstatite	78	NH_4HSO_4	1.4 M,100 °C,3 h	n.r.	75–150	29	0.3	19.6	1.50	1.89	(Sanna et al., 2014a)
[10] Serpentinite	Antigorite lizardite verculite	20	H_2SO_4	1 M, 50 °C, 2 h	n.r.	90	23.7	0.3	17.57	1.36	2.31	(Van Essendelft and Schobert, 2009)
[11] Serpentinite	Antigorite lizardite verculite	70	H_2SO_4	5 M,75 °C,2 h	n.r.	38	23.7	0.3	17.57	1.36	2.31	

n.r. = not reported.
[a] Elemental composition was not reported, therefore values of Mg, Ca, and Si for orthopyroxenes were obtained from the Ocean Discovery Program website http://www-odp.tamu.edu/publications/176_sr/chap_04/c4_t7.htm#974985.
[b] Mg, Ca, and Si values are the average between XRF and ICP-OES data, provided by the author.

2014b), lower Mg extraction efficiencies were found, even when using more active acids, such as NH_4HSO_4 (Table 6 and Fig. 6). This can be explained by the fact that these rocks have lower Σ(Mg,Ca)/Si ratio values than serpentinites. As affirmed by Lavikko and Eklund (2016), serpentinites derived from dunites are more reactive than serpentinites derived from pyroxenes. They also conclude that amphiboles and pyroxenes cannot be recommended as CCSM-appropriate materials.

As shown on Table 6, authors that have worked with serpentinite (lizardite) and pyroxenes using HCl solutions in similar conditions (Daval et al., 2013; Meyer et al., 2014) regard larger particle sizes (500–800 μm and 283 μm, respectively). Consequently, they had lower Mg extraction values. Note that their rocks had low Σ(Mg,Ca)/Si values (Table 6), so they should either have used a more concentrated acid, or applied a more intense mechanical activation in order to increase Mg extraction efficiency, as it was accomplished by Van Essendelft and Schobert (2009). The lizardite used by Daval et al. (2013) had low Mg extraction. This may have been because of the structural stability offered by the flat layers due to cationic substitution of trivalent elements. However, the Al^{3+} level reported by Daval et al. (2013) was 0.88% in the form Al_2O_3. According to Lacinska et al. (2016), lizardite 1T with low Al_2O_3 (1%) levels, lead to higher Mg extraction than lizardite 1T with high Al_2O_3 levels (2.36%). Since the lizardite used by Daval et al. (2013) had low Al_2O_3 levels, the low extraction could be caused by the large particle size of the material used (500–800 μm). When using rocks with Σ(Mg,Ca)/Si ratio values lower than 1.28 (ideal serpentinite), they should be mechanically activated more. Therefore, particle size definition is based on physicochemical properties of the material.

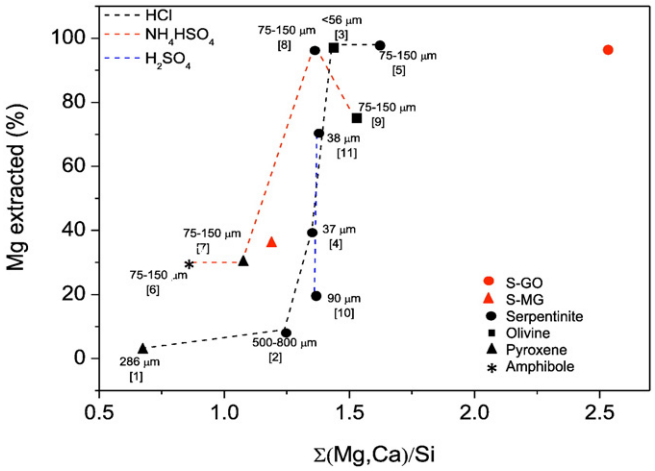

Fig. 6. Mg extraction vs. Σ(Mg, Ca)/Si from literature results. [] refers to authors on Table 6.

As observed on Fig. 6, when using NH_4HSO_4, a serpentinite with 1.37 of Σ(Mg,Ca)/Si ratio (Wang and Maroto-Valer, 2011a) was more efficient than an olivine with 1.50 of Σ(Mg,Ca)/Si ratio (Sanna et al., 2014b) although the same reaction conditions were employed. This difference can be explained by S_{BET}/V_p ratio values. Olivine has probably a low S_{BET}/V_p value, suggesting that there is less accessible surface than serpentinite, hence limiting its reactivity. However, this parameter for olivine could not be determined since the authors have not provided S_{BET} and V_p data. Future works concerning to reactivity of other silicate rocks should be studied to provide more data. For both olivines on Table 6, particle size reduction to <56 μm was enough to increase olivine reactivity (Hemmati et al., 2014a).

In this study, when mechanical activation was applied to S-MG to reduce its size to 63–75 μm, it did not increase reactivity because of its mineralogical complexity and crystal structure.

4. Conclusions

This study investigated the performance of leaching processes for use in pH swing mineral carbonation. Two different Brazilian serpentinite rocks were employed. This study also explored the

reactivity and limitations of each of them in order to evaluate Mg and Fe extraction.

Two parameters were used: the S_{BET}/V_p ratio and the Σ(Mg, Ca)/Si ratio. They are suitable to measure the resistance of these Brazilian serpentinite rocks to leaching considered the most critical step in indirect mineral carbonation. Both serpentinite rocks evaluated in this study have a reasonable R_{CO2}. However, S-MG is less reactive than S-GO, due to lower values of S_{BET}/V_p and Σ(Mg, Ca)/Si ratios than S-GO.

Results suggest that physicochemical properties determined the efficiency of Mg and Fe extraction in the leaching step, for both serpentinite rocks. S-GO and S-MG contained 8.4% and 15.3% Si into their structure; consequently, Σ(Mg,Ca)/Si ratio values were 2.64 and 1.2, respectively. Nonetheless, S_{BET}/V_p results indicate that S-GO has a larger accessible surface than S-MG for the leaching process. Consequently, Mg and Fe extraction from S-GO were 60% and 40% better than from S-MG, respectively.

Therefore, S-MG was limited not only by the low S_{BET}/V_p and Σ(Mg, Ca)/Si ratio values but also due to the crystal structure of the talc found in S-MG. The higher mineralogical complexity of S-MG reduced Mg and Fe extraction. It must be mentioned that XRD and TG/DTG analyses pointed out that Mg from talc was not leached even at high temperatures (100 °C), a high acid concentration (4 M HCl), and small particle size (75–63 μm). Talc was more stable that in other published studies because Al^{3+} is found in the structure rather than tetrahedral Si. Therefore, even when S-MG was more finely ground, the Mg was not extracted from the talc.

On the other hand, S-GO was less complex and therefore more reactive, improving Mg and Fe extraction. Mg extraction from lizardite 1T improved, even at large particle sizes (355–250 μm). This is interesting since lizardite 1T was defined as the most complex within the serpentinite group. In many cases, Mg leaching from lizardite 1T was much lower than chrysotile and antigorite (Daval et al., 2013; Sanna et al., 2013b).

For indirect mineral carbonation, low levels of trivalent elements, especially Al^{3+} in the tetrahedral sheets, higher S_{BET}/V_p and Σ(Mg,Ca)/Si values will be a determining factors in the use of the silicate rocks.

In the leaching process, the S_{BET}/V_p ratio is an indicator of the behavior of diffusion processes, just as the Σ(Mg,Ca)/Si ratio and crystal structure show the mineralogical complexity. Note that these parameters are not able to predict the extraction efficiency by themselves; however, using them provides important information that can direct the selection of material in future studies.

Acknowledgements

The authors are grateful to FAPESP for post-doctoral project number 2013/21244-5 and regular research project number 2011/19920-7 and CNPq for project number 150894/2014-7, which supported this study. The authors would also like to thank their laboratory coworkers: LCP/INPE in Cachoeira Paulista, Dr. José Augusto Jorge Rodrigues; LAS/INPE in São José dos Campos, Dr. João Paulo Barros Machado; LAI/FEG/UNESP, Dr. Luis Rogério de Oliveira Hein; LDF/CTA/ITA, Dr. Rosa Maria Rocha. In addition, the authors acknowledge the companies which provided the materials for the study: Mineração Associada (SAMA S.A.), Mineradora Pedras Congonhas Nova Lima.

Appendix A. Appendix

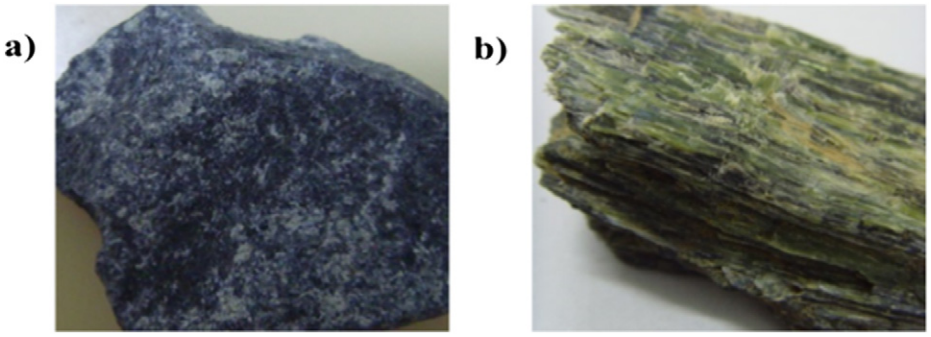

Fig. A1. Serpentinite rocks "*in natura*": (a) S-GO, (b) S-MG.

References

Alexander, G., Mercedes Maroto-Valer, M., Gafarova-Aksoy, P., 2007. Evaluation of reaction variables in the dissolution of serpentine for mineral carbonation. Fuel 86:273–281. http://dx.doi.org/10.1016/j.fuel.2006.04.034.

Arce, G.L.A.F., Carvalho Jr., J.A., Nascimento, L.F.C., 2014. A time series sequestration and storage model of atmospheric carbon dioxide. Ecol. Model. 272:59–67. http://dx.doi.org/10.1016/j.ecolmodel.2013.09.006.

Arce, G.L.A.F., Soares Neto, T.G., Ávila, I., Luna, C.M.R., Carvalho Jr., J.A., 2017. Leaching optimization of mining wastes with lizardite and brucite contents for use in indirect mineral carbonation through the pH swing method. J. Clean. Prod. 141:1324–1336. http://dx.doi.org/10.1016/j.jclepro.2016.09.204.

Assima, G.P., Larachi, F., Molson, J., Beaudoin, G., 2013. Accurate and direct quantification of native brucite in serpentine ores new methodology and implications for CO_2 sequestration by mining residues. Thermochim. Acta 566:281–291. http://dx.doi.org/10.1016/j.tca.2013.06.006.

Assima, G.P., Larachi, F., Molson, J., Beaudoin, G., 2014. Comparative study of five Québec ultramafic mining residues for use in direct ambient carbon dioxide mineral sequestration. Chem. Eng. J. 245:56–64. http://dx.doi.org/10.1016/j.cej.2014.02.010.

Azdarpour, A., Asadullah, M., Mohammadian, E., Hamidi, H., Junin, R., Karaei, M.A., 2015. A review on carbon dioxide mineral carbonation through pH-swing process. Chem. Eng. J. 279:615–630. http://dx.doi.org/10.1016/j.cej.2015.05.064.

Baba, A.A., Ibrahim, A.S., Bale, R.B., Adekola, F.A., Alabi, A.G.F., 2015. Purification of a Nigerian talc ore by acid leaching. Appl. Clay Sci. 114:476–483. http://dx.doi.org/10.1016/j.clay.2015.06.031.

Bobicki, E.R., Liu, Q., Xu, Z., Zeng, H., 2012. Carbon capture and storage using alkaline industrial wastes. Prog. Energy Combust. Sci. 38:302–320. http://dx.doi.org/10.1016/j.pecs.2011.11.002.

Bobicki, E.R., Liu, Q., Xu, Z., 2015. Mineral carbon storage in pre-treated ultramafic ores. Miner. Eng. 70:43–54. http://dx.doi.org/10.1016/j.mineng.2014.08.009.

Chang, E.E., Pan, S.Y., Chen, Y.H., Tan, C.S., Chiang, P.C., 2012. Accelerated carbonation of steelmaking slags in a high-gravity rotating packed bed. J. Hazard. Mater. 227–228:97–106. http://dx.doi.org/10.1016/j.jhazmat.2012.05.021.

Das, S., Stone, D., Convey, D., Neithalath, N., 2014. Materials characterization pore- and micro-structural characterization of a novel structural binder based on iron carbonation. Mater. Charact. 98:168–179. http://dx.doi.org/10.1016/j.matchar.2014.10.025.
Daval, D., Hellmann, R., Martinez, I., Gangloff, S., Guyot, F., 2013. Lizardite serpentine dissolution kinetics as a function of pH and temperature, including effects of elevated pCO2. Chem. Geol. 351:245–256. http://dx.doi.org/10.1016/j.chemgeo.2013.05.020.
Dri, M., Sanna, A., Maroto-Valer, M.M., 2013. Dissolution of steel slag and recycled concrete aggregate in ammonium bisulphate for CO_2 mineral carbonation. Fuel Process. Technol. 113: 114–122. http://dx.doi.org/10.1016/j.fuproc.2013.03.034.
Edenhofer, O., Pichs-Madruga, R., Sokona, Y., Minx, J.C., Farahani, E., Susanne, K., Seyboth, K., Adler, A., Baum, I., Brunner, S., Eickemeier, P., Kriemann, B., Savolainen, J., Schlomer, S., von Stechow, C., Zwickel, T., 2014. IPCC 2014: climate change 2014: mitigation of climate change. Working Group III Contribution to the Fifth Assessment Report of the Intergovernmental Panel on Climate Change http://dx.doi.org/10.1017/CBO9781107415416.
Erlund, R., Koivisto, E., Fagerholm, M., Zevenhoven, R., 2016. Extraction of magnesium from four Finnish magnesium silicate rocks for CO_2 mineralisation - part 2: aqueous solution extraction. Hydrometallurgy http://dx.doi.org/10.1016/j.hydromet.2016.07.005.
Evans, B.W., 2008. Control of the products of serpentinization by the Fe2+ Mg-1 exchange potential of olivine and orthopyroxene. J. Petrol. 49:1873–1887. http://dx.doi.org/10.1093/petrology/egn050.
Faust, G., Fahey, J., 1962. The Serpentine-Group Minerals: Geological Survey Professional Paper 384-A.
Fricker, K.J., Park, A.H.A., 2013. Effect of H_2O on $Mg(OH)_2$ carbonation pathways for combined CO_2 capture and storage. Chem. Eng. Sci. 100:332–341. http://dx.doi.org/10.1016/j.ces.2012.12.027.
Frost, R.B., Beard, J.S., 2007. On silica activity and serpentinization. J. Petrol. 48:1351–1368. http://dx.doi.org/10.1093/petrology/egm021.
Frost, B.R., Evans, K.A., Swapp, S.M., Beard, J.S., Mothersole, F.E., 2013. The process of serpentinization in dunite from New Caledonia. Lithos 178:24–39. http://dx.doi.org/10.1016/j.lithos.2013.02.002.
Gadikota, G., Natali, C., Boschi, C., Park, A.-H.A., 2014a. Morphological changes during enhanced carbonation of asbestos containing material and its comparison to magnesium silicate minerals. J. Hazard. Mater. 264:42–52. http://dx.doi.org/10.1016/j.jhazmat.2013.09.068.
Gadikota, G., Swanson, E.J., Zhao, H., Park, A.-H.A., 2014b. Experimental design and data analysis for accurate estimation of reaction kinetics and conversion for carbon mineralization. Ind. Eng. Chem. Res. 53:6664–6676. http://dx.doi.org/10.1021/ie500393h.
Gadikota, G., Fricker, K.J., Jang, S.-H., Park, A.-H.A., 2015. Carbonation of silicate minerals and industrial wastes and their potential use as sustainable construction materials. Carbon Dioxide Utilisation: Closing the Carbon Cycle, first ed. :pp. 115–137 (Washington DC). 10.1016/B978-0-444-62746-9.00008-6.
Goff, F., Guthrie, G.D., Lipin, B., Fite, M., Chipera, S., Counce, D., Kluk, E., Ziock, H., 2000. Evaluation of Ultramafic Deposites in Eastern United States and Puerto Rico as Sources of Magnesium for Carbon Dioxide Sequestration (New Mexico).
Hemmati, A., Shayegan, J., Bu, J., Yeo, T.Y., Sharratt, P., 2014a. Process optimization for mineral carbonation in aqueous phase. Int. J. Miner. Process. 130:20–27. http://dx.doi.org/10.1016/j.minpro.2014.05.007.
Hemmati, A., Shayegan, J., Sharratt, P., Yeo, T.Y., Bu, J., 2014b. Solid products characterization in a multi-step mineralization process. Chem. Eng. J. 252:210–219. http://dx.doi.org/10.1016/j.cej.2014.04.112.
Klobes, P., Klaus, M., Munro, R.G., 2006. Porosity and Specific Surface Area Measurements for Solid Materials, National I. ed. NIST - National Institute of Standards and Technology, Washington.
Lacinska, A.M., Styles, M.T., Bateman, K., Wagner, D., Hall, M.R., Gowing, C., Brown, P.D., 2016. Acid-dissolution of antigorite, chrysotile and lizardite for ex situ carbon capture and storage by mineralisation. Chem. Geol. 437:153–169. http://dx.doi.org/10.1016/j.chemgeo.2016.05.015.
Lackner, K.S., Wendt, C.H., Butt, D.P., Joyce, E.L., Sharp, D.H., 1995. Carbon dioxide disposal in carbonate minerals. Energy 20, 1153–1170.
Lavikko, S., Eklund, O., 2016. The significance of the serpentinite characteristics in mineral carbonation by "the ÅA Route". Int. J. Miner. Process. 152:7–15. http://dx.doi.org/10.1016/j.minpro.2016.04.009.
McCutcheon, J., Dipple, G.M., Wilson, S.A., Southam, G., 2015. Production of magnesium-rich solutions by acid leaching of chrysotile: A precursor to field-scale deployment of microbially enabled carbonate mineral precipitation. Chem. Geol. 413, 119–131.
Meyer, N.A., Vogeli, J.U., Becker, M., Broadhurst, J.L., Reid, D.L., Franzidis, J.P., 2014. Mineral carbonation of PGM mine tailings for CO_2 storage in South Africa: a case study. Miner. Eng. 59: 45–51. http://dx.doi.org/10.1016/j.mineng.2013.10.014.
Moore, D.E., Rymer, M.J., 2007. Talc-bearing serpentinite and the creeping section of the San Andreas fault. Nature 448:795–797. http://dx.doi.org/10.1038/nature06064.
Olajire, A.A., 2013. A review of mineral carbonation technology in sequestration of CO_2. J. Pet. Sci. Eng. 109:364–392. http://dx.doi.org/10.1016/j.petrol.2013.03.013.
Oskierski, H.C., Dlugogorski, B.Z., Jacobsen, G., 2013. Sequestration of atmospheric CO_2 in a weathering-derived, serpentinite-hosted magnesite deposit: 14C tracing of carbon sources and age constraints for a refined genetic model. Geochim. Cosmochim. Acta 122:226–246. http://dx.doi.org/10.1016/j.gca.2013.08.029.
Park, A.-H.A., Fan, L.-S., 2004. CO_2 mineral sequestration: physically activated dissolution of serpentine and pH swing process. Chem. Eng. Sci. 59:5241–5247. http://dx.doi.org/10.1016/j.ces.2004.09.008.
Power, I.M., Wilson, S.A., Dipple, G.M., 2013. Serpentinite carbonation for CO_2 sequestration. Elements 9:115–121. http://dx.doi.org/10.2113/gselements.9.2.115.
Putnis, A., 2003. Introduction to Mineral Science. Cambridge University Press, United States of America.
Ramli, M., Tabassi, A.A., Hoe, K.W., 2013. Porosity, pore structure and water absorption of polymer-modified mortars: an experimental study under different curing conditions. Compos. Part B Eng 55:221–233. http://dx.doi.org/10.1016/j.compositesb.2013.06.022.
Rayner, J.H., Brown, G., 1973. The crystal structure of talc. Clay Clay Miner. 21:103–114. http://dx.doi.org/10.1016/j.bbapap.2011.09.006.
Sanna, A., Dri, M., Hall, M.R., Maroto-Valer, M.M., 2012. Waste materials for carbon capture and storage by mineralisation (CCSM) - a UK perspective. Appl. Energy 99:545–554. http://dx.doi.org/10.1016/j.apenergy.2012.06.049.
Sanna, A., Dri, M., Maroto-Valer, M.M., 2013a. Carbon dioxide capture and storage by pH swing aqueous mineralisation using a mixture of ammonium salts and antigorite source. Fuel 114:153–161. http://dx.doi.org/10.1016/j.fuel.2012.08.014.
Sanna, A., Wang, X., Lacinska, A., Styles, M., Paulson, T., Maroto-Valer, M.M., 2013b. Enhancing Mg extraction from lizardite-rich serpentine for CO_2 mineral sequestration. Miner. Eng. 49: 135–144. http://dx.doi.org/10.1016/j.mineng.2013.05.018.
Sanna, A., Lacinska, A., Styles, M., Maroto-Valer, M.M., 2014a. Silicate rock dissolution by ammonium bisulphate for pH swing mineral CO_2 sequestration. Fuel Process. Technol. 120: 128–135. http://dx.doi.org/10.1016/j.fuproc.2013.12.012.
Sanna, A., Uibu, M., Caramanna, G., Kuusik, R., Maroto-Valer, M.M., 2014b. A review of mineral carbonation technologies to sequester CO_2. Chem. Soc. Rev. 43:8049–8080. http://dx.doi.org/10.1039/C4CS00035H.
Styles, M.T., Sanna, A., Lacinska, A.M., Naden, J., Maroto-Valer, M.M., 2014. The variation in composition of ultramafic rocks and the effect on their suitability for carbon dioxide sequestration by mineralization following acid leaching. Greenh. Gases. Sci. Technol. 4:1–12. http://dx.doi.org/10.1002/ghg.1405.
Teir, S., Kuusik, R., Fogelholm, C.-J., Zevenhoven, R., 2007a. Production of magnesium carbonates from serpentinite for long-term storage of CO_2. Int. J. Miner. Process. 85:1–15. http://dx.doi.org/10.1016/j.minpro.2007.08.007.
Teir, S., Revitzer, H., Eloneva, S., Fogelholm, C.-J., Zevenhoven, R., 2007b. Dissolution of natural serpentinite in mineral and organic acids. Int. J. Miner. Process. 83:36–46. http://dx.doi.org/10.1016/j.minpro.2007.04.001.
Temuujin, J., Okada, K., Jadambaa, T.S., MacKenzie, K.J.D., Amarsanaa, J., 2002. Effect of grinding on the preparation of porous material from talc by selective leaching. J. Mater. Sci. Lett. 21: 1607–1609. http://dx.doi.org/10.1023/A:1020373617167.
Ukwattage, N.L., Ranjith, P.G., Yellishetty, M., Bui, H.H., Xu, T., 2015. A laboratory-scale study of the aqueous mineral carbonation of coal fly ash for CO_2 sequestration. J. Clean. Prod. 103: 665–674. http://dx.doi.org/10.1016/j.jclepro.2014.03.005.
Van Essendelft, D.T., Schobert, H.H., 2009. Kinetics of acid digestion of serpentine with concurrent grinding. 1. Initial investigations. Ind. Eng. Chem. Res. 48, 2556–2565.
Van Essendelft, D.T., Schobert, H.H., 2010. Kinetics of the acid digestion of serpentine with concurrent grinding. 3. Model validation and prediction. Ind. Eng. Chem. Res. 49:1588–1590. http://dx.doi.org/10.1021/ie901159t.
Wang, X., Maroto-Valer, M.M., 2011a. Dissolution of serpentine using recyclable ammonium salts for CO_2 mineral carbonation. Fuel 90:1229–1237. http://dx.doi.org/10.1016/j.fuel.2010.10.040.
Wang, X., Maroto-Valer, M.M., 2011b. Integration of CO_2 capture and mineral carbonation by using recyclable ammonium salts. ChemSusChem 4:1291–1300. http://dx.doi.org/10.1002/cssc.201000441.
Wicks, F.J., Whittaker, E.J.W., 1975. A reappraisal of the structures of the serpentine minerals. Can. Mineral. 13, 227–243.
Yuen, Y.T., Sharratt, P.N., Jie, B., 2016. Carbon dioxide mineralization process design and evaluation: concepts, case studies, and considerations. Environ. Sci. Pollut. Res. 23:22309–22330. http://dx.doi.org/10.1007/s11356-016-6512-9.
Zeng, Q., Zhang, D., Sun, H., Li, K., 2014. Characterizing pore structure of cement blend pastes using water vapor sorption analysis. Mater. Charact. 95:72–84. http://dx.doi.org/10.1016/j.matchar.2014.06.007.